



Research Article



Biogenesis of silver nanoparticles using leaf extracts of *Asparagus racemosus* and *Sophora interrupta*: structure characterization, antibacterial and anticancer studies

Bethu Murali Satyanarayana¹ · Netala Vasudeva Reddy² · Siva kesava Rao Kommula³ · J. Venkateswara Rao¹

Received: 12 May 2020 / Accepted: 13 October 2020 / Published online: 21 October 2020
© Springer Nature Switzerland AG 2020

Abstract

The present investigation reports simple and eco-friendly biogenesis of silver nanoparticles (AgNPs) using leaf extracts of *Asparagus racemosus* and *Sophora interrupta*. UV–Vis spectra showed absorption peaks at 413 and 420 nm respectively corresponding to *A. racemosus* (AR-AgNPs) and *S. interrupta* (SI-AgNPs). TEM, DLS, XRD and TGA studies revealed that biogenic AgNPs are monodispersed, spherical shaped, thermally stable, FCC crystals and 4–15 nm in size. Zeta potential values were found to be –28.9 and –18.6 mV respectively corresponding to SI-AgNPs and AR-AgNPs. SI-AgNPs exhibited strong antibacterial activities against *Escherichia coli*, *Klebsiella pneumoniae*, *Bacillus subtilis* and *Micrococcus luteus* with inhibition zones of 11.8, 10.5, 9.8 and 9.1 mm respectively. Further SI-AgNPs exhibited significant cytotoxic properties against SKOV3, DU149, PC3 and A549 cells with IC₅₀ values of 120.87, 191.34, 235.06 and 314.27 µg/mL respectively. SI-AgNPs induce pronounced apoptotic effects on SKOV3 cells including loss of membrane integrity, chromatin condensation (pyknosis) and nuclear fragmentation (karyorrhexis). SI-AgNPs exhibited significant cell migration inhibition by reducing the wound healing of SKOV3 monolayers. Phytosynthesized AgNPs were found to be biocompatible towards normal (CHO) cells.

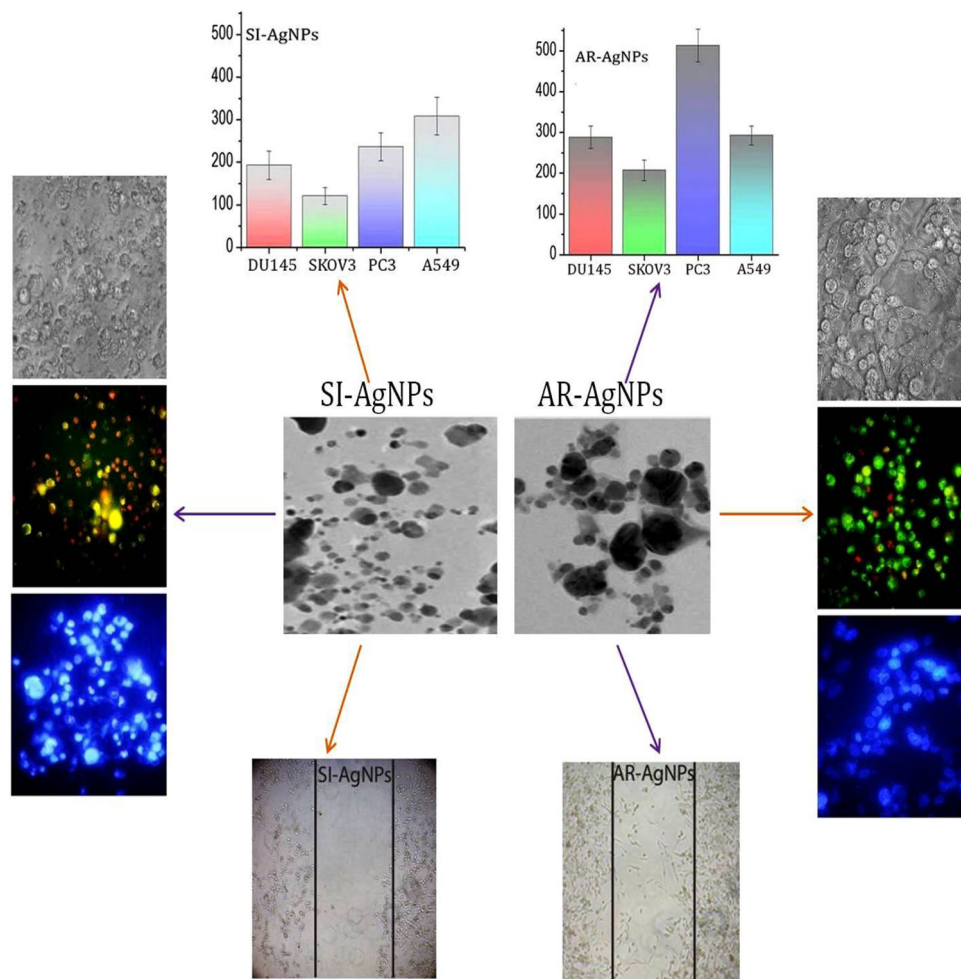
Bethu Murali Sathyanarayana and Netala Vasudeva Reddy contributed equally to this work.

✉ Bethu Murali Satyanarayana, bmurali321@gmail.com | ¹Applied Biology Division, CSIR-Indian Institute of Chemical Technology, Hyderabad, Telangana 500007, India. ²Department of Biotechnology, Sri Venkateswara University, Tirupati, Andhra Pradesh 517502, India. ³Department of Biochemistry, Dr. Y.S.R. Horticultural University, Venkataramanna Gudem, Andhra Pradesh, India.



SN Applied Sciences (2020) 2:1857 | <https://doi.org/10.1007/s42452-020-03699-7>

Graphic abstract



Keywords Silver nanoparticles · *Sophora interrupta* · Antibacterial activity · Anticancer activity · Apoptotic studies · Wound healing assay

1 Introduction

Nanotechnology has become one of the most emerging areas that intertwine all the fields of science including physics, chemistry, biology, medicine and material science [1]. Nanobiotechnology involves the eco-friendly synthesis and biomedical applications of different types of metal and metal oxide nanomaterials [2]. Metallic nanomaterials, particularly silver nanoparticles (AgNPs) have attracted global attention due to their unique physico-chemical and biological properties including optical, electronic, thermal, optoelectronic, catalytic, antimicrobial and cytotoxic properties [2–5]. Owing to their unique properties, AgNPs

have been widely employed in the various applications including optical materials [4], sensors for the detection of different chemicals, ions, pollutants and pathogens [6, 7] catalysts for the chemical reactions and dyes [8], bioprobes for enzymes [9], bioimaging and drug delivery [10, 11] and bioactive agents including antimicrobial, antioxidant, and anticancer agents [1–3, 12, 13]. The unique properties of AgNPs are determined by their size, shape, crystallinity and stability [4]. Different physical, chemical and biological methods have been employed for the preparation of stable nanomaterials with controlled size and shape [14].

Different physical and chemical approaches have been reported for the preparation of AgNPs. Notable physical

synthesis methods including laser ablation, gamma irradiation, electron irradiation and ultrasound irradiation methods [15] have been reported successfully. Different chemical synthesis methods including polyol synthesis, polyaniline synthesis, polyacrylate synthesis, polyethylene synthesis, sonochemical synthesis and reduction methods [15–18] have been widely employed for the preparation of AgNPs. Physical and chemical methods are time consuming and vast expensive. Further physical and chemically synthesized AgNPs are not clean and biocompatible as they involve toxic chemicals as coating/capping agents. Synthesizing AgNPs using plant extracts has been extensively studied and recognized as a green and efficient way for the synthesis of clean, non-toxic and biocompatible AgNPs [19, 20]. Phytochemicals of plant extracts may act as reducing and capping agents for AgNPs. The reduction methods by plant extract containing enzymes/proteins, polyphenols, flavonoids, amino acids, polysaccharides, and vitamins are eco-benign, yet chemically complex [21]. The key advantages of plant mediated synthesis (phytosynthesis) of AgNPs includes simple, eco-friendly and rapid synthesis at ambient temperatures, neutral pH, controlled size and shape characteristics, non-toxic, and increased biocompatibility [22]. Phytosynthesis of AgNPs is a bottom-up approach involving the reduction and oxidation reactions mediated by enzymes, proteins, flavonoids, polyphenols or other biomolecules with reducing properties. AgNPs have been synthesized successfully using different plant extracts including *Salvinia molesta* [3], *Berberis vulgaris* [12], *Oxalis scandens* [13], *Punica granatum* [19], *Convolvulus arvensis* [21], *Morus alba* [23], *Tithonia diversifolia* [24], *Bauhinia acuminata* [25], *Phlomis bracteosa* [26], *Tanacetum vulgare* [27], *Ficus religiosa* [28], *Mangifera indica* [29], *Nyctanthes arbor* [30], *Priva cordifolia* [31], *Artocarpus heterophyllus* [32].

Medicinal plants were collected from Seshachalam forest of Eastern Ghats, Andhra Pradesh India. The medicinal plants including *Asparagus racemosus* and *Sophora interrupta* which are abundantly available in this region and possess properties such as antibacterial, antifungal, anti-inflammatory, analgesic, antidiabetic, antipyretic, anti-septic, antioxidant and anticancer properties. All these collected species were identified by the renowned plant taxonomist at Osmania University, Hyderabad, India.

Asparagus racemosus belongs to the family Asparagaceae is commonly known as shatavari/shatamull/pilli gaddalu in Telugu. The plant grows in both the tropical and subtropical areas of India. The plant contain woody stem with small spines. The plant flowers leaving a mild fragrance in its surroundings with attractive red berry fruits. The plant is used in traditional Indian medicine for the control of stomach pain, diarrhoea, inflammation,

burning sensation, excessive perspiration, nervous debility, cough, bronchitis and skin diseases [33]. *Sophora interrupta* belongs to the family of Fabaceae and it has importance as a folk-lore medicine for preventing many ailments including cancer. It is popularly known as Adavi rela or Adavi billa in Telugu. This plant is traditionally used to treat different diseases of human health [34].

In the present study we investigate the preparation of AgNPs using leaf extracts of two plants including *A. racemosus* and *S. interrupta* collected from Seshachalam hills range of Eastern Ghats, India. The prepared biogenic AgNPs were characterized by using different spectroscopic techniques and compared the physico-chemical properties. Antibacterial properties of biogenic AgNPs were evaluated against Gram-positive and Gram-negative bacteria. Further anticancer properties of the biogenic AgNPs were evaluated against different human cancer cell lines as well as normal mammalian cells.

2 Materials and methods

2.1 Chemicals, reagents and cell lines

Two different cell culture media Dulbecco/Vogt modified Eagle's (Harry Eagle) minimal essential medium (DMEM), and Roswell Park Memorial Institute medium (RPMI-1640) were bought from Sigma-Aldrich (St. Louis, MO, USA). Fetal bovine serum was obtained from Gibco (Invitrogen), South America origin. PBS and HBSS were purchased from Sisco Research Laboratories Pvt. Ltd. (SRL)-India. Silver nitrate (AgNO_3) and all other chemicals were purchased from Sigma. The cell lines such as human ovarian carcinoma cells (SKOV3), human prostate cancer (DU145 and PC-3), human lung adenocarcinoma (A549) and Chinese hamster ovary (CHO) cell lines were obtained from the National Centre for Cellular Sciences (NCCS), Pune, India.

2.2 Preparation of leaf aqueous extracts

The dried leaves of plant species including *A. racemosus* and *S. interrupta* were grounded into fine powder and then transferred into glass jars of 1 L capacity. Initially, 100 g of dried leaf powder was added to 200 mL of autoclaved Milli-Q water. The mixture was boiled for 2–3 times (3 min each) at 30 min interval using a microwave oven (800 W, LG). During each interval, the mixture was vigorously stirred. The mixture was collected into the centrifuge tubes after boiling. The colour of the extract was pale brown and centrifuged the aqueous extract at $12,000\times g$ for 10 min. The supernatant was stored at 4 °C until further usage.

2.3 Biogenesis of AgNPs

Aqueous solution of 1 mM of AgNO₃ was prepared in Milli-Q-water. In actual experiments, the individual leaf extracts of 5 mL were added to 95 mL of 1 mM AgNO₃ solution for the reduction of Ag⁺ ions at 45 °C in a constant shaking at 500 rpm in orbital shaking incubator for 24 h. The formation of AgNPs was analyzed by UV–Vis absorption spectrophotometer with a resolution of 1 nm.

2.4 Characterization of AgNPs

The UV–Vis spectra of AgNPs synthesized by plant extracts of *A. racemosus* and *S. interrupta* was carried out between 200 and 800 nm using UV–Vis double-beam spectrometer (Spectra MAX; Molecular Devices; supported by SoftMax Pro-5.4) at a scan speed of 480 nm/min at room-temperature. After the confirmation of the synthesis, the colloidal solution of AgNPs was centrifuged at 10,000 rpm for 30 min and the obtained pellet was washed thrice with deionized water to remove unbound phytochemicals, debris and other components present in the solution and the AgNPs were dried by lyophilization to obtain a powder. This powder was stored at 4 °C for further characterization and biological studies. Fourier transform infrared (FTIR) spectrum of the dried powder of AgNPs in the form of KBr pellet was recorded on ThermoNicolet Nexus 670 spectrometer at a resolution of 4 cm⁻¹ in the wave number region of 500–4000 cm⁻¹. The crystalline structure of AgNPs was determined using X-ray diffraction (XRD) analysis. The XRD pattern of AgNPs was recorded on PANalytical Empyrean operated at a voltage of 40 kV and current of 30 mA using CuK α radiation ($\lambda = 1.5406 \text{ \AA}$). The diffractometer was controlled with data scan software using scan rate of 1.2° per minute and scan range of $2\theta = 0^\circ - 80^\circ$. Transmission electron microscope (TEM) analysis was done to determine the morphology and size of AgNPs. TEM (100 W infrared lamp JEOL JSM-2100F) was operated at an accelerating voltage of 200 kV with maximum magnification ranging from 25,000 \times – 450,000 \times . The dried AgNPs powder was redispersed in deionized water and subjected to dynamic light scattering (DLS) to determine the zeta potential on a Zetasizer Nano ZS (Malvern Instruments Ltd., UK) instrument equipped with a He–Ne laser operating at 632.8 nm and a scattering detector at 173°. Polydispersity index (PDI) value of the AgNPs was also determined using DLS. Thermo gravimetric analysis (TGA) was carried out to determine the thermal stability of AgNPs. Heating profile of 10 °C/min was used for all the tests from room temperature to 700 °C. The concentration of silver ions in the colloidal solution of AgNPs was determined by inductively coupled plasma optical emission spectrometer (ICP-OES, IRIS Intrepid II XDL, Thermo Jarrel Ash, USA). The

concentration was calculated by AgNO₃ standard graphs (1–50 ppm) plotted based on ICP-OES analysis.

2.5 Antibacterial activity of AgNPs

Different test concentrations of crude extracts and biogenic AgNPs were screened for antibacterial activity by agar disk-diffusion method [35]. Further compare the antibacterial properties of AgNPs with their respective source plant leaf extracts. The Gram-positive (*Bacillus subtilis* (MTCC 441) and *Micrococcus luteus* (MTCC 106), and Gram-negative [*Escherichia coli* (MTCC 443), and *Klebsiella pneumonia* (MTCC 109)] bacterial pathogens were obtained from Microbial Type Culture Collection and Gene bank (MTCC, Chandigarh). Test solutions were prepared using double distilled water in a 10 mL test tubes marked with a, b, c and d separately. 100 μg of crude extract was taken in Test tube 'a' and dissolved in 4 mL of water with a final concentration of 25 $\mu\text{g}/\text{mL}$. 100 μg of dried powder of AgNPs was taken in Test tube 'b' and dissolved in 4 mL of water with a final concentration of 25 $\mu\text{g}/\text{mL}$. 40 μg of standard drug (gentamycin) was taken in Test tube 'c' and dissolved in 4 mL of water with a final concentration of 10 $\mu\text{g}/\text{mL}$. Test tube 'd' contains only double distilled water. Sterile paper disks (0.7 cm) were saturated with 25 μL of each test solution and allowed to dry. For all the bacterial strains, overnight cultures were adjusted to an inoculum size of $1-2 \times 10^8$ CFU/mL. An aliquot (0.2 mL) of each inoculum was added to the molten Mueller–Hinton agar medium (HiMedia Limited) containing petriplates. Thereafter, the completely saturated disks were transferred onto the upper layer of the Mueller–Hinton agar medium inoculated with bacteria. Each petriplate contain four disks. One disk was impregnated plant extract, second disk was impregnated with AgNPs. Third disk was impregnated with standard drug gentamycin. Fourth disk contains only distilled water. Petriplates were incubated for 24 h in bacterial growth chamber to observe the growth inhibition. After incubation period of 24 h at 37 °C, antibacterial activity was evaluated by quantifying the zones of inhibition (mm) of bacterial growth (mean of six replicates was considered).

2.6 Anticancer activity of AgNPs

Anticancer activity was evaluated using the MTT [3-(4, 5-dimethylthiazol-2-yl)-2, 5-diphenyl tetrazolium bromide] assay [36]. Anticancer activity of biogenic AgNPs was evaluated against four different cancer cell lines including human ovarian carcinoma (SKOV3), human prostate cancer (PC-3 and DU145) and human lung adenocarcinoma (A549). FDA approved drug molecule doxorubicin used as a positive control. Cells were seeded in each well

containing 100 μL of medium at a final density of (2×10^4 cells/well) at identical conditions. After overnight incubation, the test compounds (leaf extracts and biogenic AgNPs) were dissolved in one mL of media. The cells were treated with different concentrations of test compounds (1–400 $\mu\text{g}/\text{mL}$). After 24 h of incubation, 10 μL of MTT (5 mg/mL) was added to each well and then the plates were incubated at 37 °C in the dark for 4 h. The formazan crystals formed were dissolved in DMSO (100 $\mu\text{L}/\text{well}$) and the reduction of MTT was quantified by absorbance at 570 nm in a spectrophotometer (Spectra MAX M2e; Molecular Devices; supported by SoftMax Pro-5.4). The data was subjected to linear regression analysis and the regression lines were plotted for the best straight-line fit. The IC_{50} (concentration that inhibit 50% of cell viability) values were calculated using the respective regression equation.

2.6.1 Study of morphological changes of cells

Morphological changes of cancer cells were observed after 24 h of treatment with IC_{50} concentrations of biogenic AgNPs (SI-AgNPs and AR-AgNPs). Morphological changes such as cell shrinkage, warping of cells, membrane blebbing and formation of apoptotic bodies were studied using phase contrast microscopy (Optika, Italy) and fluorescence microscopy [37, 38].

2.6.2 Acridine orange-Ethidium bromide staining assay

Apoptotic changes after 24 h of treatment were studied by Acridine orange-Ethidium bromide (AO-EtBr) staining assay [39]. This assay is based on the principle that the live cells will be permeable to acridine orange but not to ethidium bromide. Hence live cells will be appeared in green. While dead cells will be permeable to both acridine orange and ethidium bromide, and dead cells will be appeared in red. Briefly, 95 μL of 24 h treated cell suspension was

added to 5 μL of dye mixture at a concentration of 100 $\mu\text{g}/\text{mL}$. Then cells were washed with PBS thoroughly. After staining, cells were visualized immediately under a blue filter of fluorescence microscopy.

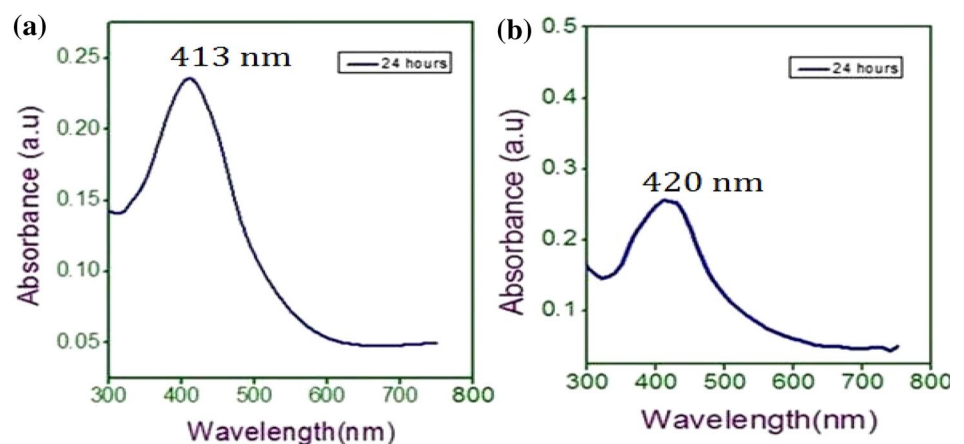
2.6.3 Hoechst staining assay

Nuclei of apoptotic cells showed very condensed chromatin. Hoechst 33,342 staining was used to detect the apoptotic nuclei [40]. Hoechst 33,342, a bis-benzimide dye binds AT-rich (Adenosine/thymidine) regions in the minor groove of ds DNA and emits very brightly. Normal cells containing loose chromatin shows moderate staining. After 24 h of treatment, cells were centrifuged and the pellet washed with PBS, and fixed the cells in 70% ethanol for 2 h. Then the cells were stained with 10 μL of Hoechst 33,342 solution (100 $\mu\text{g}/\text{mL}$ concentration). Then centrifuged the cells to remove the dye and the cells were washed finally with PBS. Nuclear morphology changes were visualized under fluorescence microscopy using excitation wavelengths between 330 and 380 nm.

2.6.4 Cell migration inhibition assay

To study the cell migration and inhibition, an in vitro wound healing assay or scratch assay is performed [41]. In this assay cells were seeded into a 24-well culture dish until 90% confluent. Then the cells were maintained in serum-free medium for 12 h. The monolayers were carefully scratched using a 200 μL pipette tip. The cellular debris was subsequently removed by washing with PBS, and the cells were incubated in serum free medium containing IC_{50} concentrations of SI-AgNPs and AR-AgNPs and without AgNPs for 24 h. The migrated cells were fixed in cold 75% methanol for 30 min and washed thrice with PBS. The cultures were photographed at 0 and 24 h to monitor the migration of cells into the wounded area.

Fig. 1 UV-Vis absorption spectra at 24 h of newly synthesized AgNPs using leaf extracts of **a** *A. racemosus* and **b** *S. interrupta*



2.7 Software tools and statistical analysis

In this study we have used Microsoft-Excel 2007 for equations and Microsoft-Word 2007 for symbols. The graphs were drawn using Prism 7.0 software. The peaks related to UV-Vis, FTIR, TGA and XRD were drawn and interpreted using Origin Pro 8.5 software. Antibacterial activity data was represented as mean of six replicates. Anticancer activity data was represented as mean ± SE of three independent experiments.

3 Results and discussion

3.1 Biogenesis of AgNPs using plant extracts

Crude aqueous leaf extracts of individual plants were prepared and the supernatants were stored at 4 °C. This extracts act as reducing and capping agents for the synthesis and stabilization of AgNPs. Initially, synthesis of AgNPs was detected by colour change of reaction solutions (containing plant leaf extract and AgNO₃) from light

yellow colour to dark brown. Further they were analyzed by UV-Vis, TEM, XRD, DLS, TGA, ICP-OES and FTIR spectroscopic techniques. Furthermore, the synthesized AgNPs were evaluated for biological properties including antimicrobial and anticancer activities.

3.2 UV-Vis analysis of biogenic AgNPs

The colloidal solution of AgNPs synthesized from leaf extracts of *A. racemosus* and *S. interrupta* exhibited maximum absorption between 410 and 430 nm corresponding to the localized surface plasmon resonance (SPR) of AgNPs. The absorption spectra of AgNPs synthesized using two plant leaf extracts for 24 h at 45 °C are presented in Fig. 1. Thus the absorption spectra indicate the formation of AR-AgNPs (*A. racemosus* leaf mediated AgNPs) and SI-AgNPs (*S. interrupta* leaf mediated AgNPs). AR-AgNPs showed maximum absorption at 413 nm and SI-AgNPs showed maximum absorption at 420 nm. It is reported earlier that absorbance around 400–430 nm is a characteristic feature of these noble metal nanoparticles [42, 43]. These biogenic AgNPs were stable for 6 months without shifting

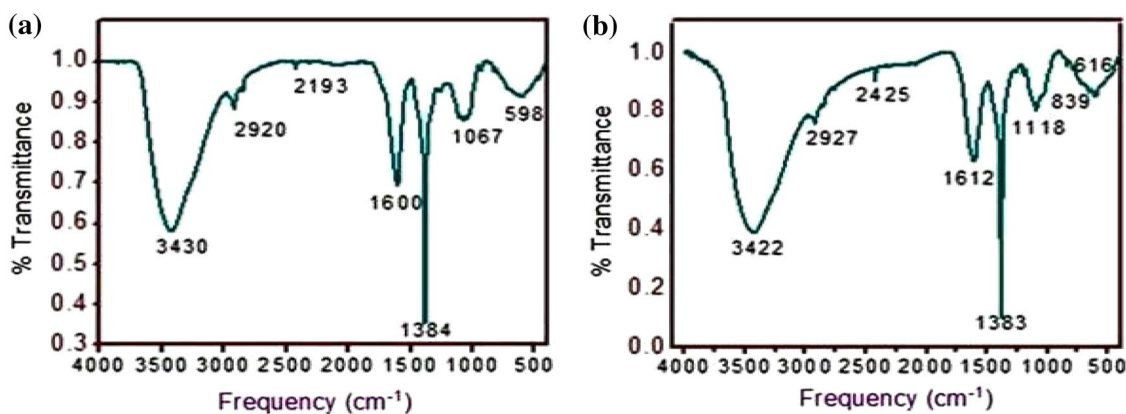
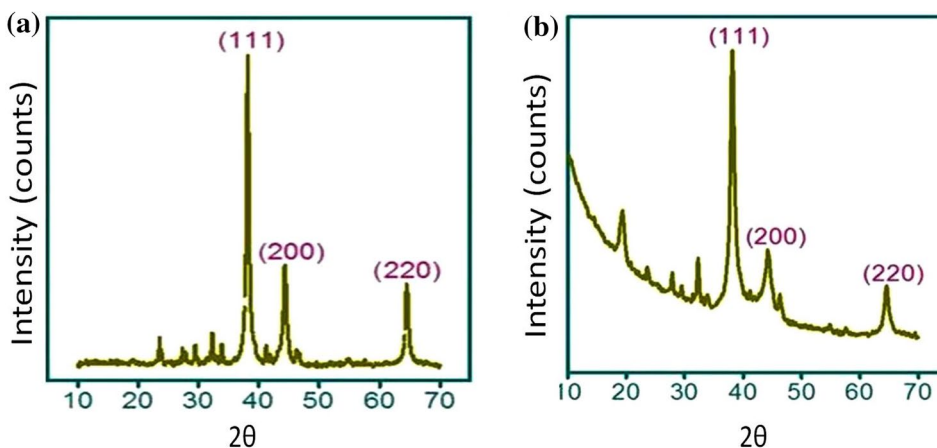


Fig. 2 FTIR spectra of **a** AR-AgNPs and **b** SI-AgNPs

Fig. 3 XRD pattern of **a** AR-AgNPs and **b** SI-AgNPs



the absorption (SPR) peak. This suggests that the phytochemicals present in this medicinal plant leaf extracts also act as capping agents which impart stabilization to AgNPs.

3.3 FTIR analysis of biogenic AgNPs

FTIR analysis was carried out to determine the functional groups involved in the synthesis and stabilization of AgNPs (Fig. 2). FTIR spectrum of AR-AgNPs (Fig. 2a) showed peaks at 598, 1067, 1384, 1600, 2193, 2920 and 3430 cm^{-1} . FTIR spectrum of SI-AgNPs (Fig. 2b) showed peaks at 616, 839, 1118, 1383, 1612, 2425, 2927 and 3422 cm^{-1} . The peaks at 3422 and 3430 cm^{-1} were corresponding to O–H group of alcohols/phenols [26]. The peaks at 2920 and 2927 cm^{-1} were corresponding to asymmetric C–H stretching vibrations of aromatic compounds such as flavonoids and phenols. This indicates that phenolic compounds of plants mainly involved in the reduction of silver ions into AgNPs. The peaks at 1600 and 1612 cm^{-1} were corresponding to

amide-II linkage of the proteins [28]. The peaks at 1383 and 1384 cm^{-1} were corresponding to C–N stretching vibrations of aromatic amines. The peaks at 1067 and 1118 were responsible for C–O stretching vibrations of phenolic acids/flavonoids/proteins [27]. This indicates that proteins of plant leaf extracts could be involved in the capping of AgNPs. The capping gives stability by preventing them from agglomeration. Further these proteins (involved in capping) and polyphenols and flavonoids (involved in bioreduction) impart biological activities to AgNPs. Thus the results of FTIR studies clearly indicated the presence of

Table 1 Zeta potential and polydispersity index (PDI) of biogenic AgNPs synthesized in the present study

AgNPs	Zeta potential (mV)	PDI
AR-AgNPs	−18.6	0.4
SI-AgNPs	−28.9	0.3

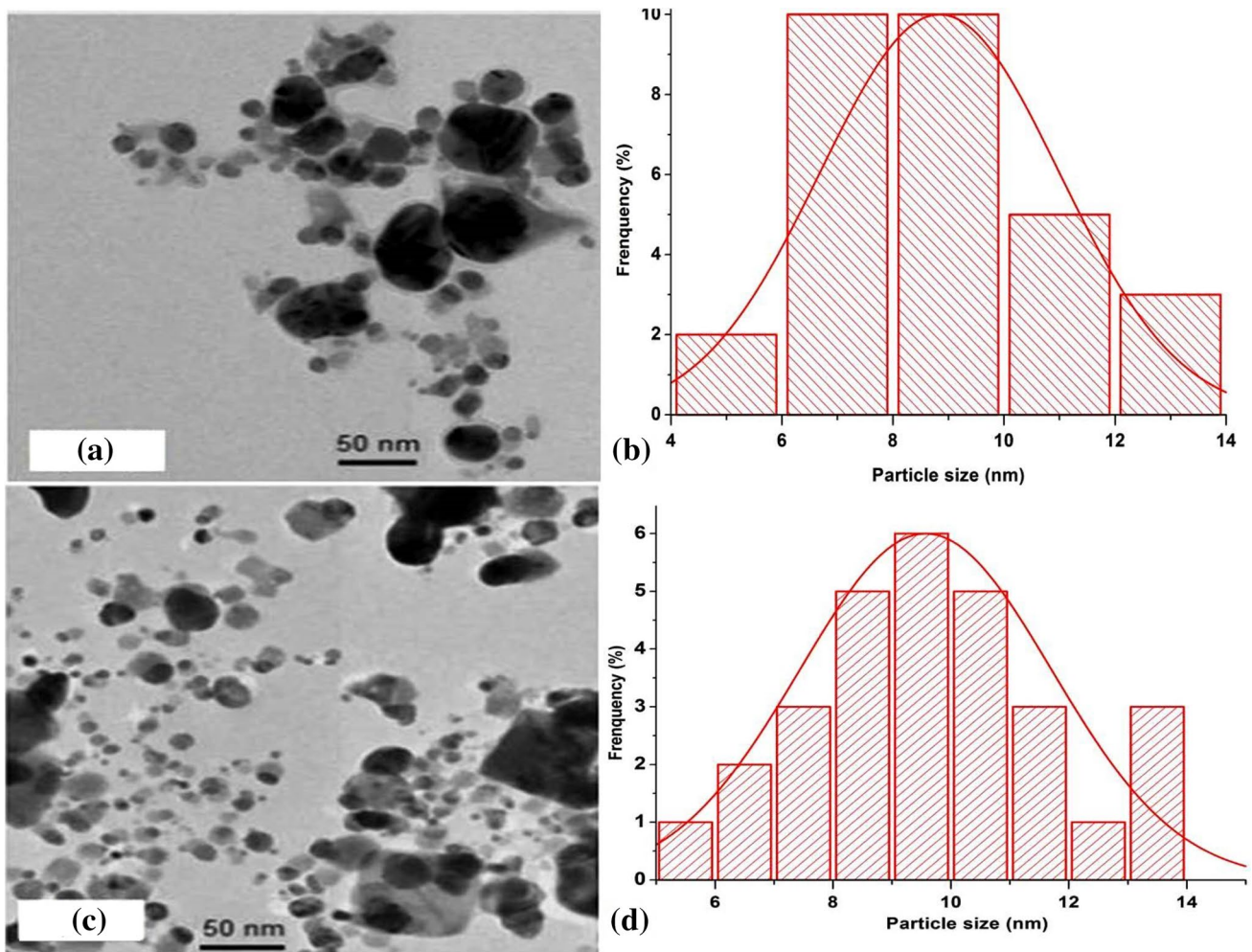


Fig. 4 TEM image AR-AgNPs (a) and corresponding histogram (b); TEM image of SI-AgNPs (c) and corresponding histogram (d)

different phytochemicals involved in the bioreduction of Ag⁺ ions into AgNPs as well as capping of AgNPs.

3.4 XRD analysis of biogenic AgNPs

The crystalline nature of biogenic AgNPs synthesized using two different plant extracts was confirmed by XRD analysis (Fig. 3). The XRD spectrum of AR-AgNPs showed three diffraction peaks at 38.17°, 44.22°, and 64.56° which are corresponding to (111), (200) and (220) planes respectively of FCC structure of AR-AgNPs. Further XRD pattern of SI-AgNPs showed Bragg's diffraction peaks at 38.16°, 44.43° and 64.61° corresponding to the planes (111) (200) and (220) of the FCC structure respectively. The diffraction peaks of AR-AgNPs and SI-AgNPs were consistent with the standard database files of JCPDS (card No 04-0783), suggesting that the synthesized AgNPs were of pure crystalline nature with FCC structure. The XRD spectra obtained from the AgNPs synthesized using two different plant extracts (*A. racemosus*, and *S. interrupta*) confirmed that they were pure crystalline in nature.

3.5 TEM and DLS analysis of biogenic AgNPs

TEM analysis of biogenic AgNPs including AR-AgNPs and SI-AgNPs was carried out to reveal their size and morphology. TEM analysis showed that AR-AgNPs, and SI-AgNPs are spherical in shape (Fig. 4a–d). The particle size distribution clearly revealed that AR-AgNPs are 5–15 nm in size with maximum distribution around 8–12 nm and SI-AgNPs are 5–14 nm in size with maximum distribution of 6–10 nm. TEM results depicted that biogenic AgNPs are monodispersed, spherical and non-aggregated. Polydispersion index (PDI) values (Table 1) calculated by DLS technique further supports the monodispersion of biogenic AgNPs.

Table 2 Antibacterial activities of different plant leaf extracts used in the present study

Plant extracts	Gram-positive		Gram-negative	
	<i>B. subtilis</i>	<i>M. luteus</i>	<i>E. coli</i>	<i>K. pneumoniae</i>
<i>S. interrupta</i>	4.6	5.3	4.6	6.3
<i>A. racemosus</i>	5.3	5.3	4.8	5.3
Stand drug	16.8	17.1	18.2	17.3

Data presented as the mean values of six replicates from two individual experiments

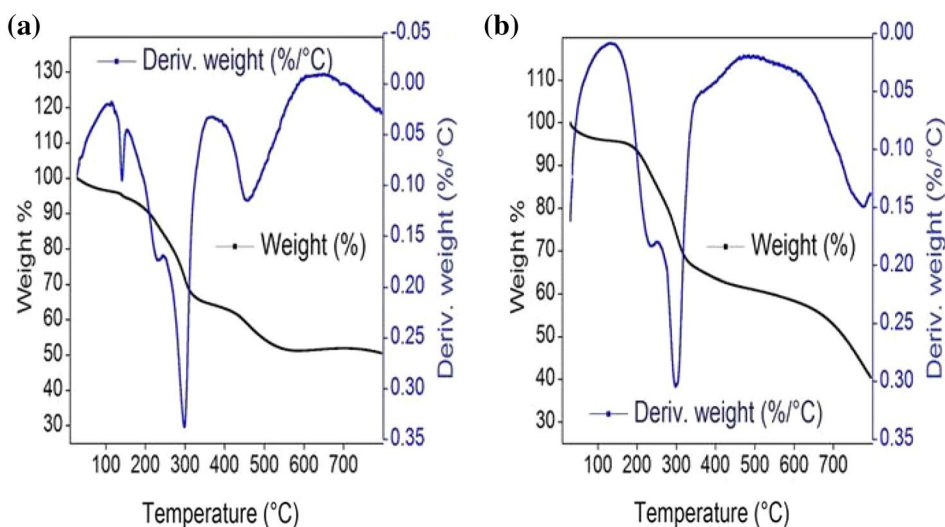
In this study, PDI values of AR-AgNPs and SI-AgNPs were found to be 0.5 and 0.3 respectively. Thus the PDI values of biogenic AgNPs were found to be below 0.7 indicating a narrow size distribution of the biogenic AgNPs. TEM results and PDI values indicated that SI-AgNPs are small in size followed by AR-AgNPs.

Zeta potential is one of the important parameter for determining the stability of the AgNPs. DLS analysis revealed the zeta potential values of the biogenic AgNPs. Zeta potential values (Table 1) of AR-AgNPs and SI-AgNPs were respectively found to be –18.6 and –28.9 mV. The high negative zeta potential values generate high repulsive forces which prevent agglomeration. It indicates that the biogenic AgNPs were long term stable without agglomeration. Based on the zeta potential value, we could say that SI-AgNPs were more stable followed by AR-AgNPs. In general, AgNPs were reported to be more stable at high negative zeta potential values.

3.6 Thermogravimetric analysis of biogenic AgNPs

TGA analysis was conducted in order to understand the thermal stability of the AR-AgNPs and SI-AgNPs. TGA plot

Fig. 5 The TGA plot of **a** AR-AgNPs and **b** SI-AgNPs



of the AR-AgNPs (Fig. 5a) exhibited three major weight losses at 230.35, 300.76, and 458.61 °C. The observed weight loss might be due to desorption of phytochemicals/bioorganic compounds capped around AgNPs. The differential thermal analysis of SI-AgNPs (Fig. 5b) revealed that maximum weight loss of 36.15% was taken place at 220–300 °C. TGA results supported that phytochemicals of plant extracts act as conjugated molecules on the surface of the AgNPs and impart stability against temperature variations. FTIR spectra also revealed that phytochemicals of plant extracts act as capping agents and give stability to the AgNPs. In this study, DLS results (high negative zeta potential) also support the stability of AgNPs.

3.7 ICP-OES analysis of biogenic AgNPs

The ICP-OES technique is used to quantify the metal content based on the emission of photons from atoms or ions that have been excited in a radio frequency discharge. AR-AgNPs showed high concentration of silver (9.26 µg/mL) followed by SI-AgNPs (6.14 µg/mL).

Based on the spectroscopic characterization, it is revealed that biogenic AgNPs were FCC crystalline in nature, spherical in shape and monodispersed. But the synthesized biogenic AgNPs were differing in their size and zeta potential measurements. SI-AgNPs were found to be very small (5–30 nm in size) compared to AR-AgNPs (10–50 nm). Further SI-AgNPs were found to show high

negative zeta potential (–28.9 mV) followed by AR-AgNPs (–18.6 mV).

3.8 Antibacterial activity of biogenic AgNPs

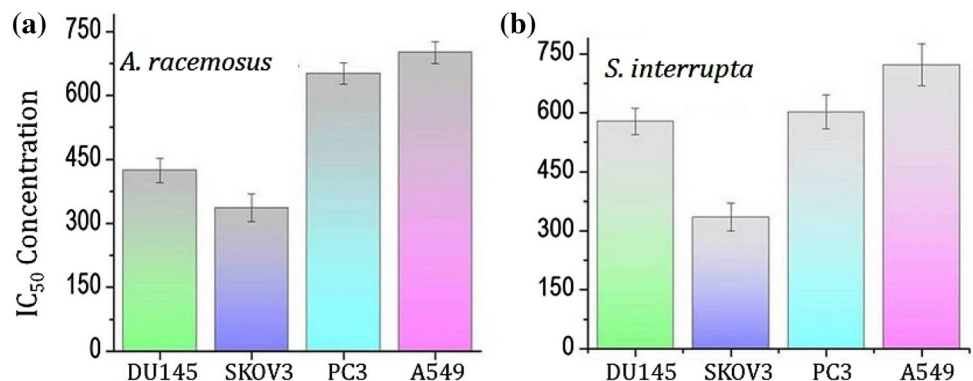
Plant aqueous crude extracts were prepared using milli-Q water and evaluated for antibacterial activities against different Gram-positive (*B. subtilis* and *M. luteus*) and Gram-negative (*E. coli* and *K. pneumoniae*) bacteria. All the extracts exhibited very well bactericidal activities at 50–100 µg/disk. To identify the potent bioactive extracts, a low concentration of 25 µg/disk was fixed. The inhibitory zone developed by the individual plant leaf extracts against each tested bacteria was measured and recorded after 24 h. The mean values of six replicates from two individual experiments are presented in Table 2. *A. racemosus* leaf extract showed effective antibacterial activity against all the tested bacteria but maximum against *K. pneumoniae* (5.3 mm). Thus the leaf extracts showed maximum antibacterial activity against *K. pneumoniae*. It is evident from the results that all the extracts produced significant zone of inhibition against all the test bacteria. Antibacterial activities of biogenic AgNPs (25 µg/disc) were evaluated against the same test strains of Gram-positive (*M. luteus* and *B. subtilis*) and Gram-negative bacteria (*E. coli* and *K. pneumoniae*) represented in Table 3. SI-AgNPs showed maximum antibacterial activity against *E. coli* (11.8 mm), followed by *K. pneumoniae* (10.5 mm), *B. subtilis* (9.8 mm) and *M. luteus* (9.1 mm). Whereas *S. interrupta* extract showed highest antibacterial activity against *K. pneumoniae* (6.3 mm) followed by *M. luteus* (5.3 mm), *B. subtilis* and *E. coli* (4.6 mm). SI-AgNPs showed 1.8–2.3 fold enhanced antibacterial activity compared to leaf extract of *S. interrupta*. AR-AgNPs exhibited effective inhibitory activity against *B. subtilis* (9.6 mm), *K. pneumoniae* (9.5 mm), *E. coli* (8.3 mm) and *M. luteus* (8.0 mm). *A. racemosus* leaf extract also showed effective antibacterial activity against all the tested bacteria including *K. pneumoniae* (5.3 mm) followed by *M. luteus* (5.3 mm), *B. subtilis* (5.3 mm) and *E. coli* (4.8 mm). AR-AgNPs exhibited 1.5–1.8 fold

Table 3 Antibacterial activities of biogenic AgNPs synthesized in the present study

AgNPs	Gram-positive		Gram-negative	
	<i>B. subtilis</i>	<i>M. luteus</i>	<i>E. coli</i>	<i>K. pneumoniae</i>
SI-AgNPs	9.8	9.1	11.8	10.5
AR-AgNPs	9.6	8.0	8.3	9.5
Stand drug	16.8	17.1	18.2	17.3

Data presented as the mean values of six replicates from two individual experiments

Fig. 6 MTT assay results confirming the in vitro cytotoxicity effects of **a** *A. racemosus* and **b** *S. interrupta* leaf extracts against different cancer cell lines. Data represented as mean ± SE of three independent experiments



highest antibacterial activities compared to leaf extract of *A. racemosus*. Thus biogenic AgNPs showed 1.5–2.5 fold enhanced antibacterial activity compared with their respective source plant leaf extract. SI-AgNPs were found to be strong antibacterial agents compared to AR-AgNPs and SI-AgNPs. In this study among all the tested bacteria, *K. pneumonia* is more susceptible to biogenic AgNPs. The difference in the susceptibility might be due to difference in their nature and composition of cell membrane as well as the interaction of AgNPs with major bacterial proteins.

Due to their antibacterial nature, AgNPs have been used in the preparation of medical kits, diagnostic kits, and other hospital accessories. Further formulations of nanosilver combined with drugs showed inhibition against multidrug resistant bacteria [44]. Formulations of nanosilver combined with drugs showed synergistic effect against microbial infections. Hence these formulations have been used for the preparations of wound dressings, wound healing ointments, and antiseptic liquids. Due to their antimicrobial nature AgNPs were also used in the preparation of water purifiers. Owing to their antimicrobial and catalytic properties, AgNPs have been used for the removal of textile dyes, microbial contaminants and other toxic contaminants from the water [45].

3.9 Anticancer activity studies

3.9.1 Cytotoxic effects of AgNPs

Leaf aqueous extracts of *A. racemosus* and *S. interrupta* were evaluated for their cytotoxic properties using MTT assay on four different human cancerous cell lines, *i.e.*, DU145, SKOV3, PC-3 and A549 (Fig. 6). Aqueous extracts of *A. racemosus*, and *S. interrupta* shown very less activity even at very high concentrations against all the cell lines. The IC_{50} values of *A. racemosus* leaf extract against DU145, SKOV3, PC-3 and A549 cell lines were respectively found to be $424.16 \pm 28.84 \mu\text{g/mL}$, $336.66 \pm 32.1 \mu\text{g/mL}$, $652.01 \pm 24.95 \mu\text{g/mL}$, and $701.14 \pm 25.43 \mu\text{g/mL}$. The

IC_{50} values of *S. interrupta* leaf extract against DU145, SKOV3, PC-3 and A549 cell lines were respectively found to be $334.81 \pm 33.7 \mu\text{g/mL}$, $602.47 \pm 35.12 \mu\text{g/mL}$, $722.69 \pm 42.81 \mu\text{g/mL}$, and $579.02 \pm 53.31 \mu\text{g/mL}$. The results revealed that all the leaf extracts showed maximum cytotoxicity against SKOV3 cells compared to other cells. Thus SKOV3 cells were found to be more susceptible compared to DU145, PC-3 and A549. The IC_{50} values of *A. racemosus* and *S. interrupta* leaf extracts against SKOV3 cells were respectively found to be $336.66 \pm 32.1 \mu\text{g/mL}$ and $334.81 \pm 33.7 \mu\text{g/mL}$. The results revealed that aqueous leaf extracts showed moderate cytotoxicity against all the cell lines used in this study. The cytotoxicity could be due to flavonoids, polyphenols, proteins and other phytochemicals present in the aqueous leaf extract.

The cytotoxic activities of the biogenic AgNPs (AR-AgNPs and SI-AgNPs) were evaluated against the cell lines including DU145, PC-3 SKOV3 and A549 (Fig. 7) Biogenic AgNPs exhibited cytotoxic activities in a concentration-dependent manner. AR-AgNPs exhibited effective cytotoxicity against SKOV3 cells ($IC_{50} = 207.1 \pm 28.9 \mu\text{g/mL}$) followed by DU145 ($IC_{50} = 286.75 \pm 30.4 \mu\text{g/mL}$), A549 ($IC_{50} = 291.37 \pm 30.4 \mu\text{g/mL}$) and PC3 ($IC_{50} = 512.34 \pm 44.5 \mu\text{g/mL}$) cells. The IC_{50} values of AR-AgNPs against different cell lines were ranging from 200 to 513 $\mu\text{g/mL}$. Whereas the IC_{50} values of *A. racemosus* leaf extract were ranging from 336 to 701 $\mu\text{g/mL}$. Thus AR-AgNPs showed to 2–3.5 fold more anticancer activity compared to pristine leaf extract, *i.e.*, *A. racemosus* leaf extract. SI-AgNPs exhibited effective cytotoxicity against SKOV3 cells ($IC_{50} = 120.87 \pm 14.9 \mu\text{g/mL}$) followed by DU145 ($IC_{50} = 191.34 \pm 20.6 \mu\text{g/mL}$), PC3 ($IC_{50} = 235.06 \pm 30.24 \mu\text{g/mL}$) and A549 ($IC_{50} = 314.27 \pm 40.6 \mu\text{g/mL}$) cells. The IC_{50} values of SI-AgNPs against different cell lines were ranging from 120 to 314 $\mu\text{g/mL}$. Whereas the IC_{50} values of *S. interrupta* leaf extract were ranging from 330 to 725 $\mu\text{g/mL}$. Thus SI-AgNPs showed 3–3.5 fold more anticancer activity compared to pristine leaf extract, *i.e.*, *S. interrupta* leaf extract. SI-AgNPs were found to be strong anticancer

Fig. 7 MTT assay results confirming the in vitro cytotoxicity effects of **a** AR-AgNPs and **b** SI-AgNPs against different cancer cell lines. Data represented as mean \pm SE of three independent experiments

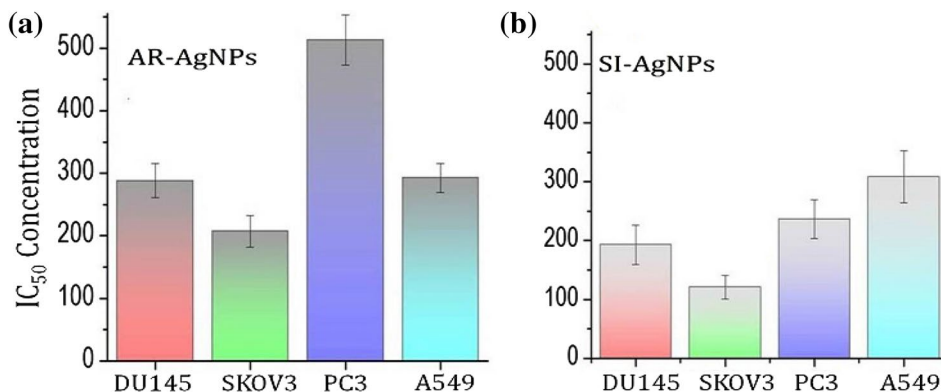
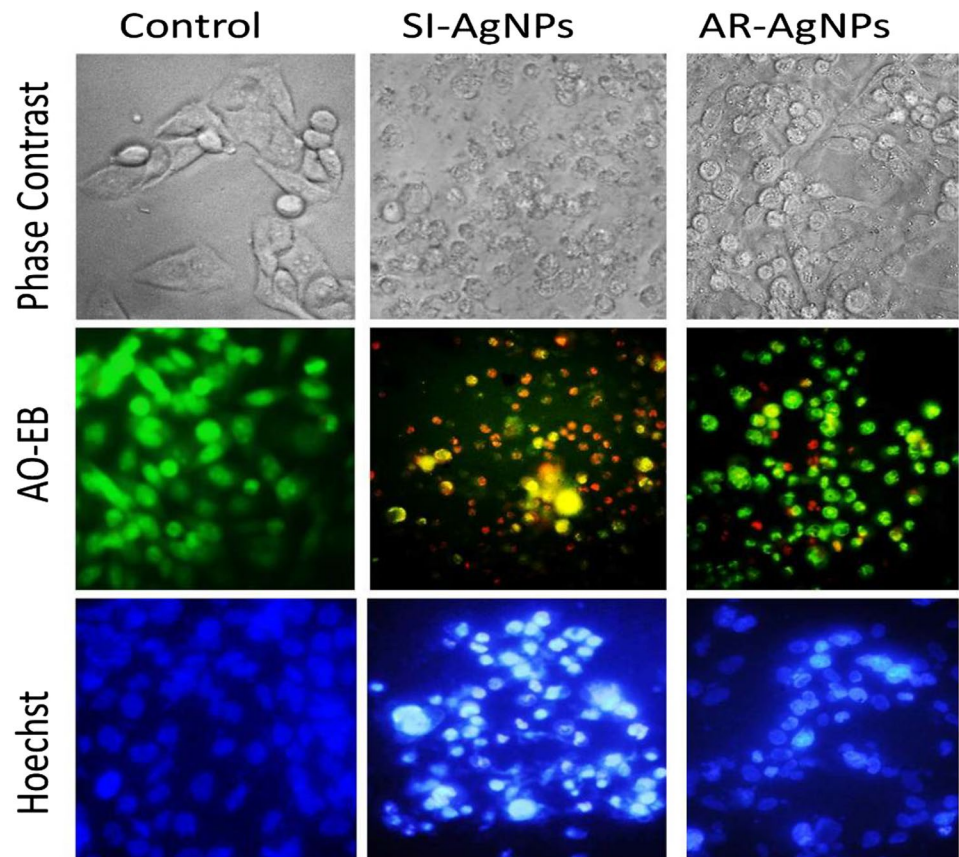


Fig. 8 Morphological changes of SKOV3 cells treated with biogenic AgNPs. Apoptotic effects of biogenic AgNPs were clearly observed in AO-EB and Hoechst staining. In AO-EB staining, viable cells appeared in green, late apoptotic cells appeared in orange shown nuclear fragmentation and loss of membrane integrity. Dead cells appeared in red colour. In Hoechst staining viable cells shown moderate staining while early apoptotic and dead cells appeared with bright fluorescence. Chromatin condensation (pyknosis) and nuclear fragmentation (karyorrhexis) were observed in early apoptotic cells

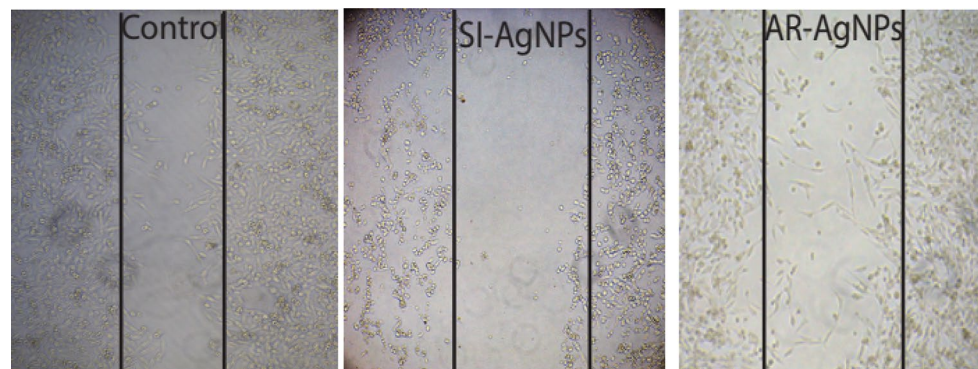


agents followed by AR-AgNPs. SI-AgNPs exhibited 1–1.5 fold more cytotoxicity than AR-AgNPs. Further the biogenic AgNPs found to show strong inhibition against SKOV3 cells. The IC_{50} values of AR-AgNPs and SI-AgNPs against SKOV3 cells were found to be 207.1 ± 28.9 and 120.87 ± 14.9 $\mu\text{g}/\text{mL}$ respectively. SKOV3 cells were found more susceptible to the biogenic AgNPs compared to other cell lines including DU145, PC3 and A549. The order of sensitivity against biogenic AgNPs among the cell lines were determined as SKOV3 > DU145 > PC-3 > A549. Further biocompatibility of the biogenic AgNPs was checked

against normal CHO cells. Nevertheless, the biogenic AgNPs are 16-fold less toxic to CHO cells.

In this study biogenic AgNPs showed more cytotoxicity compared to their respective leaf extracts. SI-AgNPs found to show more cytotoxicity compared to AR-AgNPs. Among all the cell lines used in this study, SKOV3 cells were found to be more susceptible to AgNPs compared to other cell lines including DU145, PC-3 and A549. Biogenic AgNPs showed no cytotoxicity against normal CHO cells. Hence all the biogenic AgNPs were found to be cytotoxic against cancer cells and biocompatible towards normal cells.

Fig. 9 Cell migration inhibition of SKOV3 cells treated with biogenic AgNPs. The wounded gap of SKOV3 monolayers was completely healed with cells in control. SI-AgNPs clearly decreased the healing of wounded gap and 10–15% of wounded gap only was filled with cells. AR-AgNPs showed moderate cell migration inhibition and 60–70% of wound gap was healed with cells



3.9.2 Study of morphological changes of cancer cells treated with AgNPs

Effects of biogenic AgNPs on the most susceptible cell line SKOV3 were further studied by analysing morphological changes. Apoptotic features of SKOV3 cells after 24 h of treatment with IC_{50} concentration of AgNPs were studied by phase contrast and fluorescence microscopy. General cell morphology of SKOV3 control cells (without treatment) under phase contrast and fluorescence microscopy were observed in control column. Cell morphology of SKOV3 cells after 24 h exposure to AgNPs clearly revealed the apoptotic changes (Fig. 8). In AO-EtBr staining, viable cells are permeable to acridine orange and they appeared

in green, late apoptotic cells emit orange fluorescence and they are characterized by cell membrane blebbing, cytoplasmic shrinkage, destructive fragmentation of nuclei (karyorrhexis), and irregular distribution of chromatin. While dead cells appeared in red. EtBr enters only through damaged membrane hence late apoptotic and dead cells emit orange/red fluorescence. In Hoechst staining, normal cells shown moderate staining. Early apoptotic cells had shown very bright appearance. Early apoptosis is characterized by cell shrinkage, rounding of cells, and breakdown of cytoskeleton followed by condensation of chromatin (pyknosis). AO-EtBr and Hoechst staining images clearly revealed that SI-AgNPs exhibited pronounced apoptotic effects compared to AR-AgNPs.

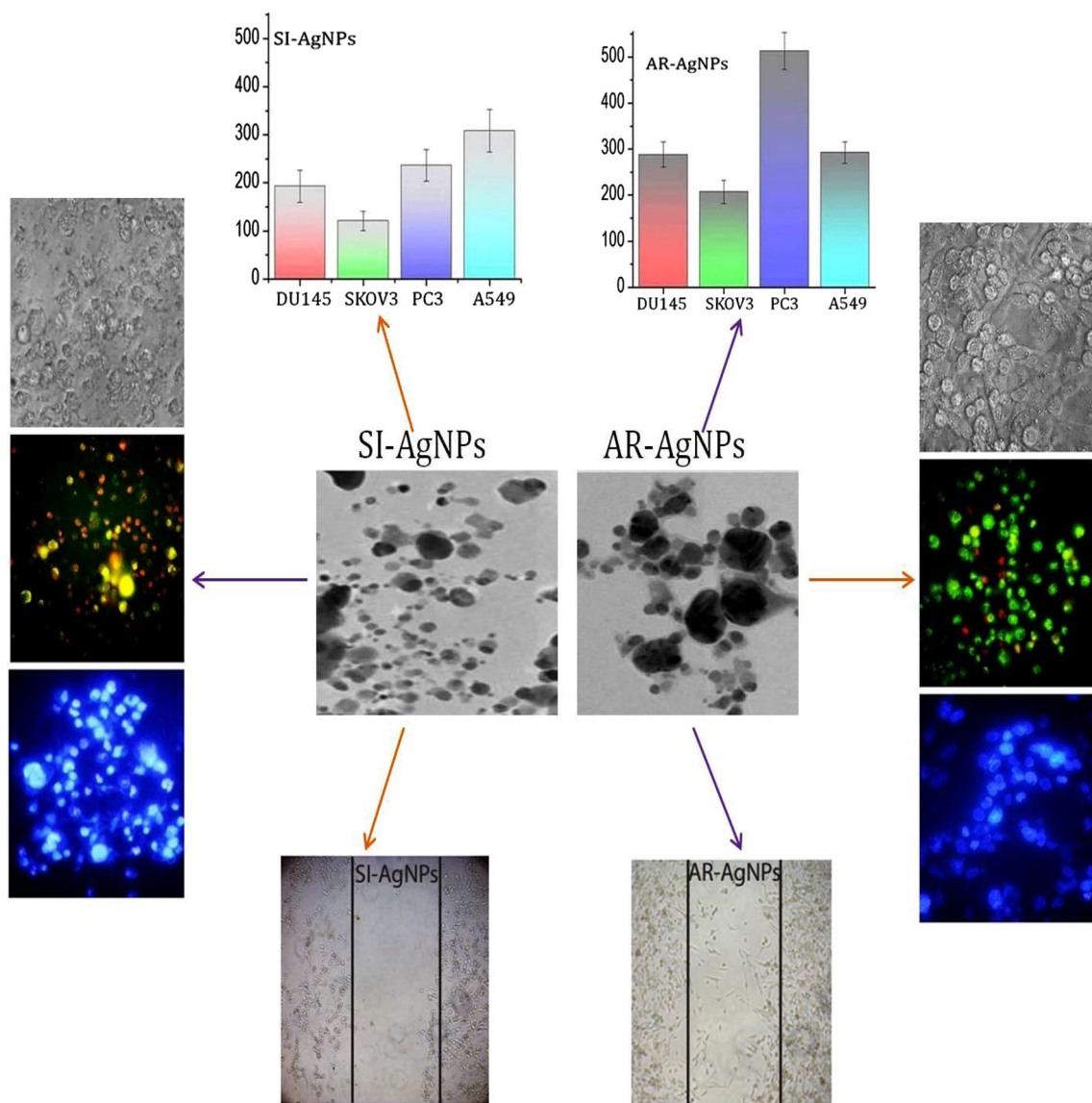


Fig. 10 Schematic representation of anticancer activity studies (MTT assay, light microscopy images, AO-EtBr staining, Hoechst staining, and cell migration inhibition) of SI-AgNPs and AR-AgNPs

Table 4 Characteristic features and biological activities of biogenic AgNPs synthesized in the present study

	AR-AgNPs	SI-AgNPs
Biosynthesis duration (h)	24	24
SPR peak (nm)	413	420
Morphology	Spherical	Spherical
Size (nm)	10–50	5–30
Crystal structure	FCC	FCC
Zeta potential (mV)	– 18.6	– 28.9
Antibacterial activity	Yes AR-AgNPs < SI-AgNPs Highest against <i>B. subtilis</i> , followed by <i>K. pneumoniae</i> , <i>E. coli</i> and <i>M. luteus</i>	Yes SI-AgNPs > AR-AgNPs Highest against <i>E. coli</i> , followed by <i>K. pneumoniae</i> , <i>B. subtilis</i> and <i>M. luteus</i>
Anticancer activity	Yes AR-AgNPs < SI-AgNPs Highest cytotoxicity against SKOV3 cells followed by DU145 A549 and PC3	Yes SI-AgNPs > AR-AgNPs Highest cytotoxicity against SKOV3 cells followed by DU145 PC3 and A549
Biocompatibility	Yes	Yes

3.9.3 Cell migration inhibition studies

Cell migration plays a key role in the progression of cancer diseases. We assessed the effects of phytosynthesized AgNPs (SI-AgNPs and AR-AgNPs) on migration ability of SKOV3 cells by wound healing/scratch assay. The results revealed that wound healing gaps are reduced clearly in control after 24 h (Fig. 9). Compared to control, phytosynthesized AgNPs reduced the closure rate of wounded area and they showed wound gaps even after 24 h. 70% of wounded area is recovered in the presence of AR-AgNPs. But, SI-AgNPs showed pronounced inhibitory effect on the cell migration and only 10 to 15% of the wounded area is recovered. Thus SI-AgNPs found to show more cytotoxic effects followed by AR-AgNPs. The inhibition of cell migration might be attributed to the decreased expression levels of matrix metalloproteinases including MMP-2 and MMP-9.

Anticancer activity studies (MTT assay, light microscopy images, AO-EtBr staining, Hoechst staining, and cell migration inhibition) of SI-AgNPs and AR-AgNPs were represented as a schematic diagram (Fig. 10).

The spectroscopic characterization features and biological activities of AR-AgNPs and SI-AgNPs were clearly represented in Table 4.

4 Conclusions

In the present study we report the successful synthesis of clean, nontoxic and biocompatible AgNPs using two plant leaf extracts including *S. interrupta* and *A. racemosus*.

The biogenic AgNPs were spherical in shape, face centered cubic crystalline in nature. The biogenic AgNPs are monodispersed with PDI value less than 0.7. The biogenic AgNPs are long term stable without agglomeration and exhibiting high negative zeta potential. SI-AgNPs were found to show strong anticancer activity and good antibacterial activity. While AR-AgNPs were moderate in both antibacterial and anticancer activities. The biogenic AgNPs showed highest cytotoxicity against SKOV3 cells followed by DU145, PC3 and A549. The biogenic AgNPs were proved to be biocompatible by showing no toxicity to normal CHO cells. In this study SI-AgNPs were found to be very small and more stable compared to AR-AgNPs. Further SI-AgNPs showed more cytotoxicity compared to AR-AgNPs. Thus the present study clearly represented the characteristic features, antibacterial and anticancer activities of AR-AgNPs and SI-AgNPs.

Authors' contributions All the work was done under the supervision of Dr. J. Venkateswara Rao and Murali Satyanarayana. N. Vasudeva Reddy carried out synthesis, characterization and manuscript preparation. Dr. Murali carried out characterization, anticancer activity and wound healing assay studies.

Compliance with ethical standards

Conflict of interest All the authors declared that they are no conflicts of interest.

Ethical statement No animals were used for the present study.

Consent for publication All the authors approved and consent for publication.

References

- Bhattacharya R, Mukherjee P (2008) Biological properties of naked metal nanoparticles. *Adv Drug Deliv Rev* 60:1289–1306
- Singh J, Dutta T, Kim K, Rawat M, Pallabi S, Kumar P (2018) Green synthesis of metals and their oxide nanoparticles: applications for environmental remediation. *J Nanobiotechnol* 16:84
- Verma DK, Hasan SH, Banik RM (2016) Photo-catalyzed and phyto-mediated rapid green synthesis of silver nanoparticles using herbal extract of *Salvinia molesta* and its antimicrobial efficacy. *J Photochem Photobiol B Biol* 155:51–59
- Kelly KL, Coronado E, Zhao LL, Schatz GC (2003) The optical properties of metal nanoparticles: the influence of size shape and dielectric environment. *J Phys Chem B* 107:668–677
- West JL, Halas NJ (2000) Applications of nanotechnology to biotechnology. *Curr Opin Biotechnol* 11:215
- Fatima M, Hassan RYA, Silvana A (2017) Multifunctional nanotechnology-enabled sensors for rapid capture and detection of pathogens. *Sensors (Basel)* 17(9):2121
- Po-Hsuan H, Chia-Yun C (2019) Insights for realizing ultrasensitive colorimetric detection of glucose based on carbon/silver core/shell nanodots. *ACS Appl Bio Mater* 2(6):2528–2538
- Ping-Tsung H, Yu-Ning C, Kuan-Chung C, Shun-Huei W, Ching-Ping L (2019) Confinement of silver nanoparticles in polystyrenes through molecular entanglements and their application for catalytic reduction of 4-nitrophenol. *J Mater Chem A* 7(36):20919–20925
- Sunfengda S, Xiaojun H, Hongjie L, Jialin Z, Kwangnak K, Hongxia C (2018) Guests involved CB[8] capped silver nanoparticles as a means of electrochemical signal enhancement for sensitive detection of caspase-3. *Sens Actuators B Chem* 274:54–59
- Neng Y, Tang BZ, Wen-Xiong W (2018) *In vivo* bioimaging of silver nanoparticle dissolution in the gut environment of zooplankton. *ACS Nano* 12:12212–12223
- Parveen S, Misra R, Sahoo SK (2012) Nanoparticles: a boon to drug delivery therapeutics diagnostics and imaging. *Nanomed Nanotechnol Biol Med* 8(2):147–166
- Behravan M, Hossein PA, Naghizadeh A, Ziaee M, Mahdavi R, Mirzapour A (2019) Facile green synthesis of silver nanoparticles using *Berberis vulgaris* leaf and root aqueous extract and its antibacterial activity. *Int J Biol Macromol* 124:148–154
- Mukherjee S, Chowdhury D, Rajesh K, Patra S, Vinothkumar B, Manika PB, Sreedhar B, Patra CR (2014) Potential theranostics application of bio-Synthesized silver nanoparticles (4-in-1 System). *Theranostics* 4:316–335
- Evanoff DD, Chumanov G (2004) Size-controlled synthesis of nanoparticles 1“silver-only” aqueous suspensions via hydrogen reduction. *J Phys Chem B* 108:13948–13956
- Abbasi AR, Kalantary H, Yousefi M, Ramazani A, Morsali A (2012) Synthesis and characterization of Ag nanoparticles@polyethylene fibers under ultrasound irradiation. *Ultrason Sonochem* 19:853–857
- Zhang Z, Patel RC, Kothari R, Johnson CP, Friberg SE, Aikens PA (2000) Stable silver clusters and nanoparticles prepared in polyacrylate and inverse micellar solutions. *J Phys Chem* 104:1176–1182
- Pastoriza-Santos I, Liz-Marzán LM (1999) Formation and stabilization of silver nanoparticles through reduction by NN-dimethylformamide. *Langmuir* 15:948–951
- Frattini A, Pellegrini N, Nicastro D, deSanctis O (2005) Preparation of amine coated silver nanoparticles using triethylenetetramine. *Mater Chem Phys* 94:148–152
- Nasiriboroumand M, Montazer M, Barani H (2018) Preparation and characterization of biocompatible silver nanoparticles using pomegranate peel extract. *J Photochem Photobiol B Biol* 179:98–104
- Vankar PS, Shukla D (2012) Biosynthesis of silver nanoparticles using lemon leaves extract and its applications for antimicrobial finish on fabric. *Appl Nanosci* 2(2):163–168
- Hamed S, Shojaosadati SA, Mohammadi A (2017) Evaluation of the catalytic antibacterial and anti-biofilm activities of the *Convolvulus arvensis* extract functionalized silver nanoparticles. *J Photochem Photobiol B Biol* 167:36–44
- Iravani S (2011) Green synthesis of metal nanoparticles using plants. *Green Chem* 13:2638–2650
- Das D, Ghosh R, Mandal P (2019) Biogenic synthesis of silver nanoparticles using S1 genotype of *Morus alba* leaf extract: characterization, antimicrobial and antioxidant potential assessment. *SN Appl Sci* 1:498
- Thi T, Thuy T, Thi T, Hu V, Thi HN (2013) Biosynthesis of silver nanoparticles using *Tithonia diversifolia* leaf extract and their antimicrobial activity. *Mater Lett* 105:220–223
- Hu D, Gu X, Si W, Qin W, Jiao J, Hao YF (2019) Biosynthesis of Silver nanoparticles using *Bauhinia acuminata* flower extract and their effect to promote osteogenesis of MSCs and improve meniscus injury healing. *J Photochem Photobiol B Biol* 197:111536
- Anjum S, Abbasi BH (2016) Biomimetic synthesis of antimicrobial silver nanoparticles using in vitro-propagated plantlets of a medicinally important endangered species: *Phlomis bracteosa*. *Int J Nanomed* 11:1663–1675
- Dubey SP, Lahtinen M, Sillanpää M (2010) Tansy fruit mediated greener synthesis of silver and gold nanoparticles. *Process Biochem* 45:1065–1071
- Kantrao S, Venkataraman A (2014) Biosynthesis and characterization of stable silver nanoparticles using *Ficus religiosa* leaf extract: a mechanism perspective. *J Clust Sci* 25:1157–1171
- Yang N, Li W-H (2013) Mango peel extract mediated novel route for synthesis of silver nanoparticles and antibacterial application of silver nanoparticles loaded onto non-woven fabrics. *Ind crop Prod* 48:81–88
- Basu S, Maji P, Ganguly J (2016) Rapid green synthesis of silver nanoparticles by aqueous extract of seeds of *Nyctanthes arbor-tristis*. *Appl Nanosci* 6:1–5
- Ananda AP, Krishnamurthy NB, Savitha KR, Nagendra BS (2019) Biogenic synthesis of silver nanoparticles using *Priva cordifolia* leaf extract (PC@AgNPs) a potent antioxidant, antibacterial and catalytic activity. *SN Appl Sci* 1:800
- Umesh BJ, Vishwas AB (2013) Green synthesis of silver nanoparticles using *Artocarpus heterophyllus* Lam seed extract and its antibacterial activity. *Ind crop Prod* 46:132–137
- Alok S, Jain SK, Verma A, Kumar M, Mahor A, Monika S (2013) Plant profile phytochemistry and pharmacology of *Asparagus racemosus* (Shatavari): a review. *Asian Pac J Trop Dis* 3:242–251
- Manjula C, Ammani K (2012) Phytochemical analysis and pharmacological importance of *Sophora interrupta* leaves. *Int J Res Pharm Biomed Sci* 3:1798–1804
- Bauer AW, Kirby WM, Sherris JC, Turck M (1966) Antibiotic susceptibility testing by a standardized single disk method. *Am J Clin Pathol* 45:493–496
- Mosmann T (1983) Rapid Colorimetric assay for cellular growth and survival: application to proliferation and cytotoxicity assays. *J Immunol Methods* 65:55–63
- Murali SB, Reddy NV, Latha D et al (2018) Potential anticancer activity of biogenic silver nanoparticles using leaf extract of *Rhynchosia suaveolens*: an insight into the mechanism. *Artif Cells Nanomed Biotechnol* 46:104–114. <https://doi.org/10.1080/21691401.2017.1414824>
- Netala VR, Murali SB, Bobbu PL et al (2016) Biogenesis of silver nanoparticles using endophytic fungus *Pestalotiopsis*

- microspora* and evaluation of their antioxidant and anticancer activities. *Int J Nanomed* 11:5683–5696
39. Shailaja KK, Amarante-Mendes GP, Finucane D, Brunner T, Bossy-Wetzel E, Green DR (2006) Acridine orange/ethidium bromide (AO/EB) staining to detect apoptosis. *Cold Spring Harb Protoc.* <https://doi.org/10.1101/pdb.prot4493>
 40. Lema C, Varela-Ramirez A, Renato JA (2011) Differential nuclear staining assay for high-throughput screening to identify cytotoxic compounds. *Curr Cell Biochem* 1:1–14
 41. Rodriguez LG, Wu X, Guan JL (2005) Wound-healing assay. *Methods Mol Biol* 294:23–29
 42. Mulvaney P (1996) Surface plasmon spectroscopy of nanosized metal particles. *Langmuir* 12:788–800
 43. Wiley BJ, Im SH, Li ZY, Mclellan J, Siekkinen A, Xia Y (2006) Maneuvering the surface plasmon resonance of silver nanostructures through shape-controlled synthesis. *J Phys Chem* 110:15666–15675
 44. Khatoon N, Alam H, Khan A, Raza K, Sardar M (2019) Ampicillin silver nanoformulations against multidrug resistant bacteria. *Sci Rep* 9:6848. <https://doi.org/10.1038/s41598-019-43309-0>
 45. Khatoon N, Alam H, Manzoor N, Sardar M (2018) Removal of toxic contaminants from water by sustainable green synthesized non-toxic silver nanoparticles. *IET Nanobiotechnol* 12:1090–1096

Publisher's Note Springer Nature remains neutral with regard to jurisdictional claims in published maps and institutional affiliations.